

## MASS AND ORBIT DETERMINATION FROM TRANSIT TIMING VARIATIONS OF EXOPLANETS

DAVID NESVORNÝ<sup>1</sup> AND ALESSANDRO MORBIDELLI<sup>1,2</sup>

Received 2008 June 20; accepted 2008 July 29

### ABSTRACT

The timing variations of transits of an exoplanet provide means of detecting additional planets in the system. The short-period and resonant variations of the transit signal are probably the most diagnostic of the perturbing planet's mass and orbit. The method can be sensitive to small perturbing masses near the transiting planet and for orbits at mean motion resonances. It is not evident, however, how the mass and orbit of the perturbing planet can be determined from the observed variations of transit times. This is a difficult inverse problem. Direct  $N$ -body integrations are computationally too expensive to provide an adequate sampling of parameter space. Here we develop an alternative method based on analytic perturbation theory. We find that this new method is typically  $\sim 10^4$  times faster than direct  $N$ -body integrations. The perturbation theory that we use here has an adequate precision to predict timing variations for most planetary orbits except those with very large eccentricities where the expansion of the disturbing function is divergent. By applying the perturbation method to the inverse problem we determine the number and precision of the measured transit times that are required for the unique and correct characterization of the perturbing planet. We find that the required precision is typically a small fraction ( $\sim 15\%$ – $30\%$ ) of the full transit timing variation amplitude. Very high precision observations of transits will therefore be needed. We discuss the optimal observation strategy to characterize a planetary system from the transit timing variations. We find that the timing of secondary transits, if measured with adequate precision, can help to alleviate the problem with the degeneracy of solutions of the inverse problem.

*Subject headings:* celestial mechanics — planetary systems

### 1. INTRODUCTION

The goal of this paper is to describe a method that could be used to determine planetary masses and orbits for exoplanetary systems where at least one of the planets is transiting over the disk of its host star. To define the problem, we assume that the parameters of the transiting planet such as its mass, semimajor axis, and eccentricity are known from the radial velocity measurements, and that a second planet gravitationally perturbs the orbital motion of the transiting planet and produces observable short-period variation in the timing of individual transits (Agol et al. 2005; Holman & Murray 2005). We then investigate how the parameters of the perturbing planet, such as its mass and orbit, can be determined from the observed transit timing variations (TTVs).

This is a difficult (inverse) problem. The simplest approach would be to use direct  $N$ -body integrations of a large sample of planetary systems (Steffen & Agol 2005; Agol & Steffen 2007) in an attempt to directly fit the observed TTV signal. This method, however, is extremely CPU expensive due to the large number of unknown parameters. In the simplest case, where the transiting planet has a near-zero eccentricity and the orbits are assumed to be coplanar, the three basic parameters of the perturbing planet that one would like to know are its mass, semimajor axis, and eccentricity. In addition, the TTV signal also depends on the orbital phase of the perturbing planet (as defined by the longitude at given epoch) and its longitude of pericenter. Because the pericenter longitude of the perturbing planet may precess (e.g., due to presence of additional planets exterior to it), we must include in the list of unknown parameters not only its initial phase but also its precession frequency. Therefore, there are six unknown parameters in total in

this case. If, for example, 50 values are needed to resolve each of the six dimensions of parameter space, more than  $10^{10}$  planetary systems would need to be tracked in total.

To speed up this calculation we develop a new method that avoids the need for extensive orbital integrations. The method is based on perturbation theory (Hori 1966; Deprit 1969). We calculate the transit time at any given epoch as a sum over Fourier terms with amplitudes and phases that are explicit functions of the unknown parameters. Our tests demonstrate that this method is typically  $\sim 10^4$  times faster than direct orbital integrations. It allows us to calculate 100 transit times for  $10^{10}$  planetary systems in about a day of CPU time.

We describe the new method in § 2 and test its precision in § 3. In § 4, we simulate synthetic TTVs with precise  $N$ -body integrations and attempt to determine the mass and orbit of the perturbing planet from them by the least-squares fit. We discuss the uncertainty of the best-fit parameters as a function of the observed number of transits, observational time base, orbit, and mass of the perturbing planet. The code described here is available on request.

### 2. METHOD

The TTV signal is a series of transit times,  $t(j)$ , with  $1 \leq j \leq N$ , where  $N$  is the total number of observed transits. The orbit period of the transiting planet,  $P_1$ , can be estimated from this data by linear regression. When  $P_1$  is extracted from  $t(j)$ , we end up with variation  $\delta t(j) = t(j) - jP_1$  that describes the difference of  $t(j)$  from a strictly periodic (i.e., single-frequency) signal. This variation can be produced by additional planets in the system that gravitationally perturb the orbit of the transiting planet and advance or delay individual transits.

The dynamics of interacting planets can be complex. Probably the most diagnostic signatures for the TTV method are the short-period and (near-) resonant oscillations of the transiting planet's orbit produced by gravitational perturbations from other planets

<sup>1</sup> Department of Space Studies, Southwest Research Institute, 1050 Walnut Street., Suite 400, Boulder, CO 80302.

<sup>2</sup> Observatoire de la Côte d'Azur, Boulevard de l'Observatoire, BP 4229, 06304 Nice Cedex 4, France.

(Holman & Murray 2005; Agol et al. 2005).<sup>3</sup> Due to these perturbations, the true longitude of the transiting planet,  $\theta_1$ , can slightly lead or trail the one of the unperturbed Keplerian orbit at the time of transit, therefore producing the timing variation. For an elliptic orbit,  $\theta_1$  can be written as a function of the mean longitude,  $\lambda_1$ , as

$$\theta_1 = \lambda_1 + \sum_{k=1}^{\infty} H_k(e_1) \sin k(\lambda_1 - \varpi_1), \quad (1)$$

where  $e_1$  and  $\varpi_1$  are the eccentricity and pericenter longitude of the transiting planet, and  $H_k(e_1)$  are polynomials in  $e_1$  with the lowest power of  $H_k$  in  $e_1$  being  $k$ . Therefore, the TTV signal may arise from changes in  $\lambda_1$ ,  $e_1$ , or  $\varpi_1$ . In practice, the eccentricity of transiting planets is typically small (Torres et al. 2008) because orbits have been circularized by tidal effects. To the lowest order in  $e_1$ , equation (1) becomes

$$\theta_1 = \lambda_1 + 2e_1 \sin(\lambda_1 - \varpi_1) + \mathcal{O}(e_1^2). \quad (2)$$

In regularized variables,  $h_1 = e_1 \sin \varpi_1$  and  $k_1 = e_1 \cos \varpi_1$ ; this leads to

$$n_1 \delta t = \delta \lambda_1 + 2\delta k_1 \sin(\lambda_1) - 2\delta h_1 \cos(\lambda_1) + \mathcal{O}(e_1), \quad (3)$$

where  $n_1$  is the mean motion of the transiting planet, and  $\delta \lambda_1$ ,  $\delta k_1$ , and  $\delta h_1$  denote the short-period variations of the osculating orbital elements. For simplicity, we do not explicitly list terms  $\mathcal{O}(e_1)$  in the above equation. These and higher order terms can be easily taken into account if  $e_1$  is significant.

In the following, we will assume that  $m_1, m_2 \ll m_0$ , where  $m_0$ ,  $m_1$ , and  $m_2$  are masses of the star, inner (transiting), and outer planets, respectively, and determine the short-period variations in  $\delta \lambda_1$ ,  $\delta h_1$ , and  $\delta k_1$  using the perturbation theory. The Hamiltonian  $H$  of the two planets orbiting a central star is

$$H = H_0 + H_1, \quad (4)$$

where

$$H_0 = -\frac{Gm_0 m_1}{2a_1} - \frac{Gm_0 m_1}{2a_2} \quad (5)$$

and

$$H_1 = -Gm_1 m_2 \left[ \frac{1}{|\mathbf{r}_1 - \mathbf{r}_2|} - \frac{\mathbf{r}_1 \cdot \mathbf{r}_2}{r_2^3} \right], \quad (6)$$

where  $G$  is the gravitational constant,  $\mathbf{r}_1$  and  $\mathbf{r}_2$  are the Jacobi coordinates of planets, and  $a_1$  and  $a_2$  are their semimajor axes (e.g., Brouwer & Clemence 1961).

We use the expansion of  $H_1$  in the Fourier series:

$$H_1 = -\frac{Gm_1 m_2}{a_2} \sum C_k^{l,j}(\alpha) e_1^{l_1} e_2^{l_2} \left( \sin \frac{i_1}{2} \right)^{j_1} \left( \sin \frac{i_2}{2} \right)^{j_2} \times \exp \iota(k_1 \lambda_1 + k_2 \lambda_2 + k_3 \varpi_1 + k_4 \varpi_2 + k_5 \Omega_1 + k_6 \Omega_2) \quad (7)$$

<sup>3</sup> The long-term effects such as the apsidal precession produced by the perturbing planet are more difficult to detect via TTVs if transit observations span only a few years (Heyl & Gladman 2007). In addition, these effects can be masked by contributions to the apsidal precession from the oblateness of the central star, relativity, and tides.

with  $\iota = \sqrt{-1}$ ,  $C_k^{l,j}(\alpha) = C_{-k}^{l,j}(\alpha)$ ,  $\alpha = a_1/a_2 < 1$ , and multi-indexes  $\mathbf{l} = (l_1, l_2)$ ,  $\mathbf{j} = (j_1, j_2)$ , and  $\mathbf{k} = (k_1, k_2, k_3, k_4, k_5, k_6)$ . Properties of equation (6) imply that  $\sum_{n=1}^6 k_n = 0$ , and that  $j_1 + j_2$ ,  $l_1 - |k_3|$ ,  $l_2 - |k_4|$ ,  $j_1 - |k_5|$ , and  $j_2 - |k_6|$  are even integers. The lowest combined power of eccentricities and inclinations that appears in front of each Fourier term in equation (7) is thus  $l_1 + l_2 + j_1 + j_2 = \sum_{n=3}^6 |k_n| \geq 0$  (see, e.g., Morbidelli 2002, pp. 35–36).

It is convenient to write equations (5) and (6) in terms of canonical Poincaré variables:

$$\begin{aligned} L_j &= m_j \sqrt{Gm_0 a_j}, & \lambda_j & \\ y_j &= \sqrt{2P_j} \cos p_j, & x_j &= \sqrt{2P_j} \sin p_j \\ z_j &= \sqrt{2Q_j} \cos q_j, & v_j &= \sqrt{2Q_j} \sin q_j, \end{aligned} \quad (8)$$

where

$$\begin{aligned} P_j &= L_j \left( 1 - \sqrt{1 - e_j^2} \right), & p_j &= -\varpi_j \\ Q_j &= L_j \sqrt{1 - e_j^2} (1 - \cos i_j), & q_j &= -\Omega_j. \end{aligned} \quad (9)$$

The indexes  $j = 1$  and  $j = 2$  denote the variables of the inner and outer planets, respectively, and  $i_j$  and  $\Omega_j$  are their inclinations and nodal longitudes. By substituting the Poincaré variables in equation (4) we find that

$$H = H_0(L_1, L_2) + H_1(L_j, y_j, z_j, \lambda_j, x_j, v_j) \quad (10)$$

with  $H_1 \ll H_0$  for  $m_1, m_2 \ll m_0$ . We do not list the expressions for  $H_0$  and  $H_1$  in the Poincaré variables here. In fact, it is not necessary to calculate these expressions explicitly because our computer algebra code can easily deal with the transformation between the orbital elements and Poincaré variables, and thus combine equations (5)–(9) to obtain equation (10).

The perturbation theory (Hori 1966; Deprit 1969) allows us to select a canonical transformation from  $E_j$  to  $\bar{E}_j$ , where  $E$  denotes arbitrary Poincaré variable, that transforms  $H$  to the new Hamiltonian,  $\bar{H}$ , that does not depend on new coordinates  $\bar{\lambda}_j$ . The new momenta,  $\bar{L}_j$ , become constants of motion and  $\bar{\lambda}_j = n_j t + \lambda_j^{(0)}$ , where constants  $n_j$  and  $\lambda_j^{(0)}$  denote the mean orbital frequency of planet  $j$  and initial phase angle, respectively.

The transformation between  $E_j$  and  $\bar{E}_j$  can be given in terms of generating function  $\chi$  as

$$E_j = \bar{E}_j + \sum_{n=1}^{\infty} \frac{1}{n!} \mathcal{L}_\chi^n \bar{E}_j, \quad (11)$$

where  $\mathcal{L}_\chi^n$  is the Lie derivative defined in terms of Poisson brackets as

$$\begin{aligned} \mathcal{L}_\chi^1 \bar{E}_j &= \{ \bar{E}_j, \chi \}, \\ \mathcal{L}_\chi^n \bar{E}_j &= \mathcal{L}_\chi^1 \mathcal{L}_\chi^{n-1} \bar{E}_j. \end{aligned} \quad (12)$$

Therefore, to the first order in  $m_2/m_0$ , the terms of equation (11) relevant to equation (3) are

$$\begin{aligned} \lambda_1 &= \bar{\lambda}_1 + \frac{\partial \chi_1}{\partial \bar{L}_1}, \\ x_1 &= \bar{x}_1 + \frac{\partial \chi_1}{\partial \bar{y}_1}, \\ y_1 &= \bar{y}_1 - \frac{\partial \chi_1}{\partial \bar{x}_1}, \end{aligned} \quad (13)$$

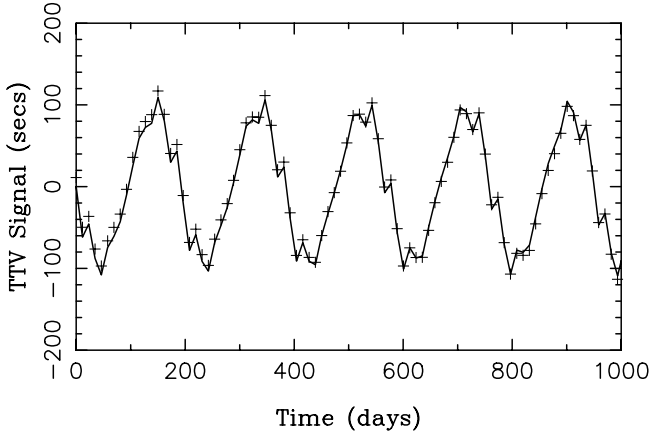


FIG. 1.— Comparison between the TTV signal determined from a precise numerical integration (*plus signs*) and the one obtained from the PT method (*solid line*). The transiting planet has  $a_1 = 0.1$  AU and  $e_1 = 0$ . The perturbing planet has  $m_2 = 10^{-4}m_0$ ,  $a_2 = 0.2$  AU, and  $e_2 = 0.1$ . The precision of the perturbation theory is good in this case. The amplitude and QPT of the TTV signal are 234 s and 2.6% (see main text for the definition of QPT).

where  $\chi_1$  denotes the first-order (linear) terms of  $\chi$  in  $m_2/m_0$ . Explicit relations between  $\delta k_1$ ,  $\delta h_1$  and  $\delta x_1 = x_1 - \bar{x}_1$ ,  $\delta y_1 = y_1 - \bar{y}_1$  can be given from the definition of these variables. With  $H_1$  defined in equation (7),  $\chi_1$  can be written as

$$\begin{aligned} \chi_1 = & \frac{Gm_1m_2}{\bar{a}_2} \sum_{|k_1|+|k_2|\neq 0} \iota \frac{C_k^{l,j}(\bar{\alpha})}{k_1n_1 + k_2n_2} \bar{e}_1^{l_1} \bar{e}_2^{l_2} \left( \sin \frac{\bar{i}_1}{2} \right)^{j_1} \\ & \times \left( \sin \frac{\bar{i}_2}{2} \right)^{j_2} \exp \iota (k_3\bar{\omega}_1 + k_4\bar{\omega}_2 + k_5\bar{\Omega}_1 + k_6\bar{\Omega}_2) \\ & \times \exp \iota (k_1\bar{\lambda}_1 + k_2\bar{\lambda}_2), \end{aligned} \quad (14)$$

where  $\bar{a}_2$ ,  $\bar{\alpha} = \bar{a}_1/\bar{a}_2$ ,  $\bar{e}_j$ ,  $\bar{i}_j$ ,  $\bar{\omega}_j$ ,  $\bar{\Omega}_j$ ,  $\bar{\lambda}_j$  are functions of the new (mean) canonical momenta and coordinates.

Series in equation (14) is not convergent for  $k_1n_1 + k_2n_2 \approx 0$ , i.e., near mean motion resonances between the two planets. To deal with this complication we eliminate all Fourier terms from equation (14) with  $k_1n_1 + k_2n_2 < n_2f_{\text{cut}}$ , where  $f_{\text{cut}}$  is the cutoff parameter. Different values of  $f_{\text{cut}}$  are tested in § 3.

According to equation (13), we must take the derivative of  $\chi_1$  with respect to  $L_1$ ,  $x_1$ , and  $y_1$ . For example, we have for  $e_1 = i_1 = 0$  that

$$\frac{\partial \chi_1}{\partial \bar{L}_1} = \frac{\partial \bar{a}_1}{\partial \bar{L}_1} \frac{\partial \chi_1}{\partial \bar{a}_1} \quad (15)$$

with

$$\frac{\partial \bar{a}_1}{\partial \bar{L}_1} = \frac{2\sqrt{\bar{a}_1}}{m_1\sqrt{Gm_0}}. \quad (16)$$

Generating function  $\chi_1$  depends on  $\bar{a}_1$  via  $C_k^{l,j}(\bar{a}_1/\bar{a}_2)$  and  $n_1$ . The corresponding derivative term is

$$\frac{\partial}{\partial \bar{a}_1} \left[ \frac{C_k^{l,j}(\bar{\alpha})}{k_1n_1 + k_2n_2} \right] = \frac{1}{k_1n_1 + k_2n_2} \left( \frac{\partial C_k^{l,j}}{\partial \bar{a}_1} - \frac{k_1 C_k^{l,j}}{k_1n_1 + k_2n_2} \frac{\partial n_1}{\partial \bar{a}_1} \right) \quad (17)$$

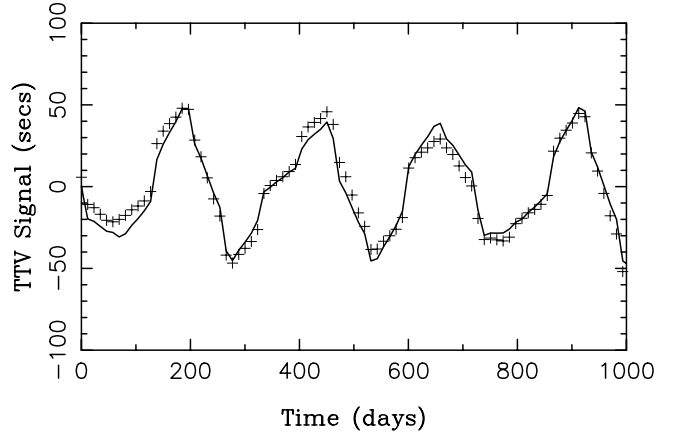


FIG. 2.— Same as Fig. 1, but for  $a_2 = 0.32$  AU and  $e_2 = 0.35$ . This case tests the precision of the perturbation theory for a large orbital eccentricity of the perturbing planet. The amplitude and QPT of the TTV signal are 104 s and 5.4%.

with

$$\frac{\partial n_1}{\partial \bar{a}_1} = -\frac{3}{2} \frac{\sqrt{Gm_0}}{\bar{a}_1^{5/2}}. \quad (18)$$

The derivatives of  $\chi_1$  with respect to  $x_1$  and  $y_1$  can also be explicitly given. We do not list them here.

There are two alternative expressions for coefficients  $C_k^{l,j}$  that we can use: (1) in terms of Laplace coefficients  $b_{s/2}^{(l)}(\alpha)$  (e.g., Ellis & Murray 2000); (2) in power series of  $\alpha$  (e.g., Kaula 1962). These expressions are equivalent as Laplace coefficients can be expanded in power series of  $\alpha$ . The domain of convergence of these series is given by the Sundman criterion (Sundman 1916), which postulates that the series is absolutely convergent for

$$a_2g(e_1) > a_1f(e_2), \quad (19)$$

where

$$g(e_1) = \sqrt{1 + e_1^2} \cosh w + e_1 + \sinh w, \quad (20)$$

$$f(e_2) = \sqrt{1 + e_2^2} \cosh z - e_2 - \sinh z \quad (21)$$

with  $w = e_1 \cosh w$  and  $z = e_2 \cosh z$ . For example, for  $\alpha = 0.5$  and  $e_1 = 0$  the expansion is convergent for  $e_2 < 0.32$ . This limits the applicability of our method. We discuss this issue in more detail in § 3.

### 3. TESTS

The perturbation theory method (hereafter the PT method) described in the previous section has been implemented in C and Fortran computer codes. The C-language code (Šidlichovský 1990) was used to calculate a table of coefficients  $C_k^{l,j}$  (and their derivatives with respect to  $\alpha$ ) for 8000 values of  $\alpha$  between 0.1 and 0.9. The code efficiently evaluates the power expansion of  $C_k^{l,j}$  in  $\alpha$  (Kaula 1962) with the maximum power selected in such a way that the numerical values of  $C_k^{l,j}$  are precise to at least seven decimal digits. For  $\alpha \sim 0.9$ , this required accounting for powers up to  $\sim 300$ . To assure that the PT method is valid for moderate to large values of  $e_2$ , we used terms  $e_2^{l_2}$  in equation (7) up to  $l_2 = 15$ . We verified that increasing the truncation order does not significantly improve the results. Our Fortran code reads the table of coefficients  $C_k^{l,j}$  (and  $dC_k^{l,j}/d\alpha$ ) and determines  $\delta t$  (eq. [3]) according to the PT method described in § 2. While our codes are capable of dealing with the case of nonzero inclinations, here we only discuss

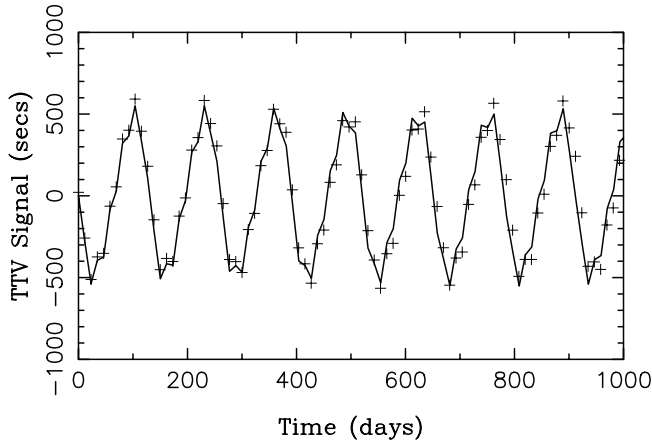


FIG. 3.— Same as Fig. 1, but for  $a_2 = 0.15$  AU and  $e_2 = 0.05$ . This case tests the precision of the perturbation theory for a compact planetary system. The amplitude and QPT of the TTV signal are 1180 s and 6.5%.

the results for  $i_1 = i_2 = 0$ . We also limit the analysis to  $e_1 \sim 0$ . Discussion of results for a more general case is left for elsewhere.

We performed the following experiments to test the precision of the PT method. In each test, we fixed the values of  $m_0$ ,  $m_1$ , and  $m_2$  and started a large number of exact  $N$ -body integrations with different initial orbits of the two planets. We assumed that the inner planet is transiting and the outer planet is gravitationally perturbing the inner planet. Their orbits were set to be coplanar. The orbit evolution was followed for a fixed timespan,  $0 < t < T_{\text{int}}$ , with the Bulirsh-Stoer integrator (Press et al. 1992). During this timespan we interpolated for and recorded all transit times of the inner planet. The same initial orbits were then used to determine the transit times from the PT method. We typically used  $T_{\text{int}} = 1000$  days in these tests. The best results were obtained with  $f_{\text{cut}} = 0.1$ – $0.2$ .

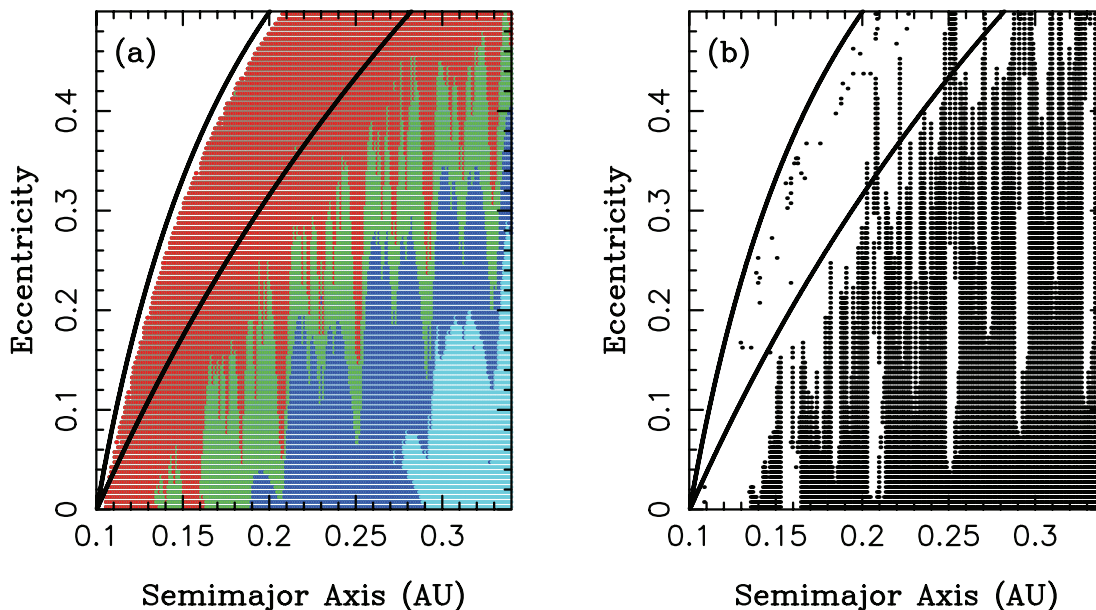


FIG. 4.— Results of the orbital survey. We placed a transiting planet on a circular orbit with  $a = 0.1$  AU from a Sun-mass star. The orbit was gravitationally perturbed by an outer planet with mass  $m_2 = 10^{-4}m_0$ . The orbits of transiting and perturbing planets were assumed to be coplanar. Semimajor axis and eccentricity of the outer planet were then varied. In each case, we numerically integrated the orbit evolution for 1000 days and registered times of 87 (primary) transits of the inner planet. (a) shows the  $(a_2, e_2)$  values that are color coded according to the amplitude of the TTV signal,  $(\delta t)_{\text{amp}}$ . The color coding is the following:  $(\delta t)_{\text{amp}} > 1000$  s (red),  $100 < (\delta t)_{\text{amp}} < 1000$  s (green),  $10 < (\delta t)_{\text{amp}} < 100$  s (blue), and  $1 < (\delta t)_{\text{amp}} < 10$  s (turquoise). The PT method described in § 2 was used to determine the transit times. We used  $f_{\text{cut}} = 0.1$  here. (b) shows the  $(a_2, e_2)$  values for which the fractional error of transit timings obtained from the PT method was better than 15%. The upper and lower solid curves in both panels show the planet-crossing and Laplacian-series convergence thresholds, respectively.

To start with, we considered a case with  $m_0 = M_{\text{Sun}}$  and  $a_1 = 0.1$  AU. Parameters  $m_2$ ,  $a_2$ , and  $e_2$  were varied to test the precision of the perturbation method for different planetary systems. Figures 1, 2, and 3 show a comparison of the TTV signals for  $a_2 = 0.2$  AU and  $e_2 = 0.1$  (case 1),  $a_2 = 0.32$  AU and  $e_2 = 0.35$  (case 2), and  $a_2 = 0.15$  AU and  $e_2 = 0.05$  (case 3). We used  $m_2 = 10^{-4}m_0$  in all these cases.<sup>4</sup> While case 1 represents the perturbing planet's orbit with moderate eccentricity and separation from the transiting planet, cases 2 and 3 are slightly more extreme. Case 2 tests the precision of the PT method for a large eccentricity of the perturbing planet. Case 3 tests it for a compact planetary system.

To quantify the precision of the PT method we define a quality parameter, QPT, as a ratio between the rms of the TTV difference between the  $N$ -body and PT methods and the amplitude of the TTV signal. According to Figures 1–3, the PT method shows a satisfactory precision for all three cases described above with QPT ranging between 2% and 7%. This result is encouraging.

Figure 4 helps us to understand the extent of the orbital space domain where the PT method performs well and where it does not.<sup>5</sup> There are two failure modes. The first one occurs when the pericenter distance of the outer planet,  $q_2 = a_2(1 - e_2)$ , approaches  $a_1$ . The PT method fails in this case because the expansion of the perturbing function is not convergent beyond the limits given by the Sundman's criterion (bottom solid lines in Fig. 4). This limitation of the PT method, however, is not as critical as it might seem because planets with  $q_2 \sim a_1$  may not be stable. To check

<sup>4</sup> We used  $m_2 = 10^{-3}m_0$  and  $m_2 = 10^{-5}m_0$  in our additional tests. We found that the amplitude of the TTV signal scales nearly linearly with  $m_2$  as it should because of the linear dependence on  $m_2$  in the PT method. We therefore do not need to extensively test different values of  $m_2$ .

<sup>5</sup> This figure was obtained with  $m_2 = 10^{-4}m_0$ . Similar surveys were done for  $m_2 = 10^{-3}m_0$  and  $m_2 = 10^{-5}m_0$ . Due to linear scaling  $\delta t$  with  $m_2$  we found that the overall pattern in Fig. 4b is nearly invariant to changes of  $m_2$ .

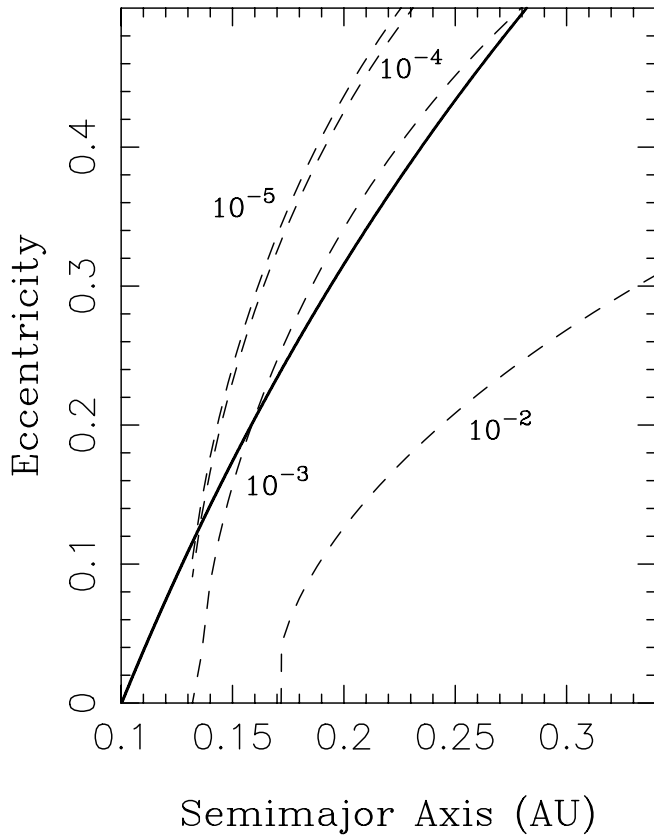


FIG. 5.—Hill stability domain for different masses of the perturbing planet. The dashed lines denote the upper boundary of the region of Hill-stable orbits according to Gladman (1993). Different curves are denoted by ratio  $m_2/m_0$ . In all cases we used  $m_0 = M_{\text{Sun}}$ ,  $m_1 = 10^{-3}m_0$ , and  $a_1 = 0.1$  AU. The solid line shows the convergence limit of the Laplacian expansion of the disturbing function as given by Sundman (1916).

on this, we plot in Figure 5 the Hill stability domain as defined by Gladman (1993). We find that the size of the problematic region, where the Laplacian expansion is divergent but the orbits are Hill stable, depends on the masses of the two planets. With  $m_1 = 10^{-3}m_0$  and  $m_2 = 10^{-5}m_0$  this region opens with increasing  $a_2$  and spans a high-eccentricity strip about 0.1 wide in  $e_2$  for large  $a_2$ . On the other hand, the problematic domain vanishes for  $m_1 = m_2 \approx 10^{-3}m_0$ .

The second failure mode of the PT method occurs at the mean motion resonances between the two planets. Specifically, the vertical gaps in Figure 4b where the precision of the PT method degrades correspond to resonances such as the 2 : 1 at 0.159 AU, 3 : 1 at 0.208 AU, 4 : 1 at 0.252 AU, 5 : 1 at 0.294 AU, and 6 : 1 at 0.33 AU. Figure 6a illustrates an example of TTVs for planets in the 4 : 1 mean motion resonance. In this example, the TTV signal is a wave with period  $\approx 850$  days. It is produced by the resonant oscillations of the planetary orbits. Due to these oscillations, the semimajor axis of the transiting planet varies and affects  $n_1$ . Accordingly,  $\lambda_1$  has a variable rate and can significantly lead or trail that of the unperturbed orbit. This motion propagates into the TTV signal via equation (3). The resonant modes are not taken into account in the PT method, as explained in § 2 (they must be removed from eq. [14] to avoid divergence of  $\chi_1$ ).

In Figure 7, we enlarge the region near the 4 : 1 planetary resonance. It is apparent from this plot the PT method fails for  $0.2475 < a < 0.256$  AU and  $e > 0.05$ . This includes the region of resonant orbits and a narrow strip of the nonresonant orbits on each side of the 4 : 1 resonance. The performance of the PT method

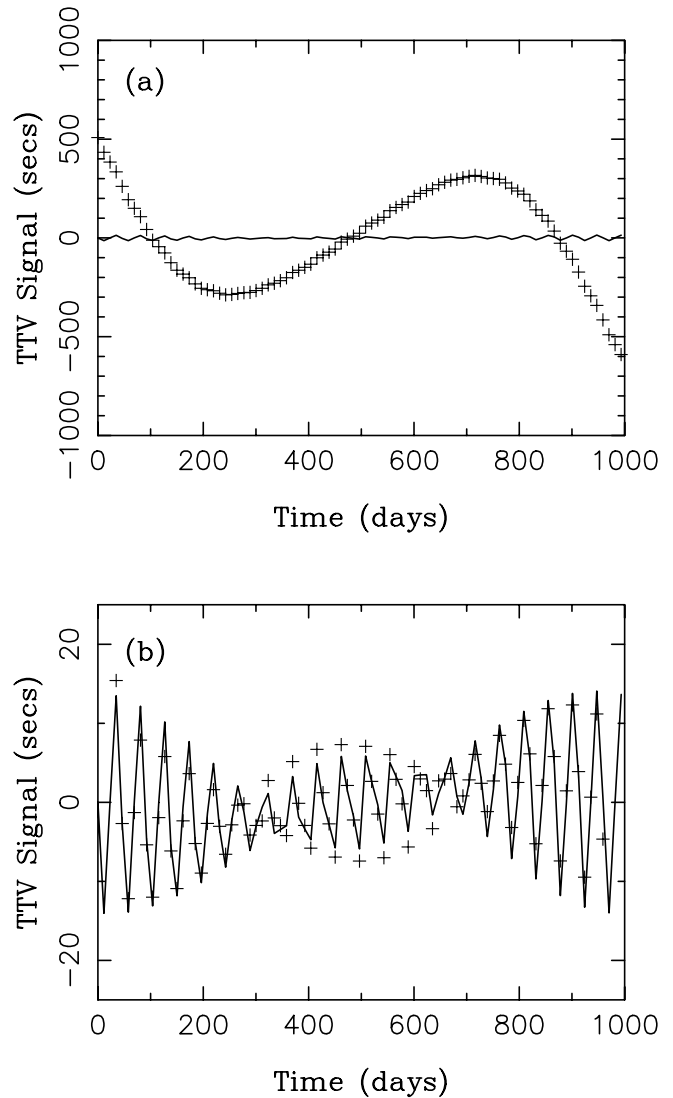


FIG. 6.—Comparison between the synthetic TTV signal (*plus signs*) and transit times obtained from the PT method (*solid lines*). As in Fig. 1, the transiting planet was set to have  $a = 0.1$  AU and  $e_1 = 0$ . In this example, the perturbing planet was set to have  $m_2 = 10^{-4}m_0$ ,  $a = 0.25$  AU, and  $e_1 = 0.2$ . This orbit is located in the 4 : 1 mean motion resonance with the transiting planet. The long-period wave shown in (a) ( $\approx 850$  days) is produced by resonant oscillations. The PT method fails to reproduce this behavior because it does not properly account for dynamics of resonant planets. In (b), we show the underlying short-period TTV signal for the same planetary system. Specifically, all frequencies with periods longer than 100 days were removed by the high-pass Fourier filter. The short-period TTVs obtained from the PT method nicely match those produced by the exact numerical simulation. The amplitude and QPT of the TTV signal in (b) are 32.8 s and 12.5%.

for near-resonant orbits can be improved using a higher-order perturbation theory (i.e., including more terms in eq. [11]). This will help to shrink the problematic region in Figure 7. We leave the development of the higher-order PT method for future work.

The failure of the PT method at the mean motion resonances does not appear to be immediately critical in practice because the resonant oscillations of the TTV signal can be characterized (and become useful) only with a long time baseline of the TTV observations. Moreover, the short-period oscillations in the underlying signal can be correctly modeled by the PT method even in the resonant case (Fig. 6b). Therefore, if any long-term variations of the TTV signal become apparent for a given system, the following method of analysis can be used. In the first step, the long-period terms can be separated from the rest by a Fourier-based filter.

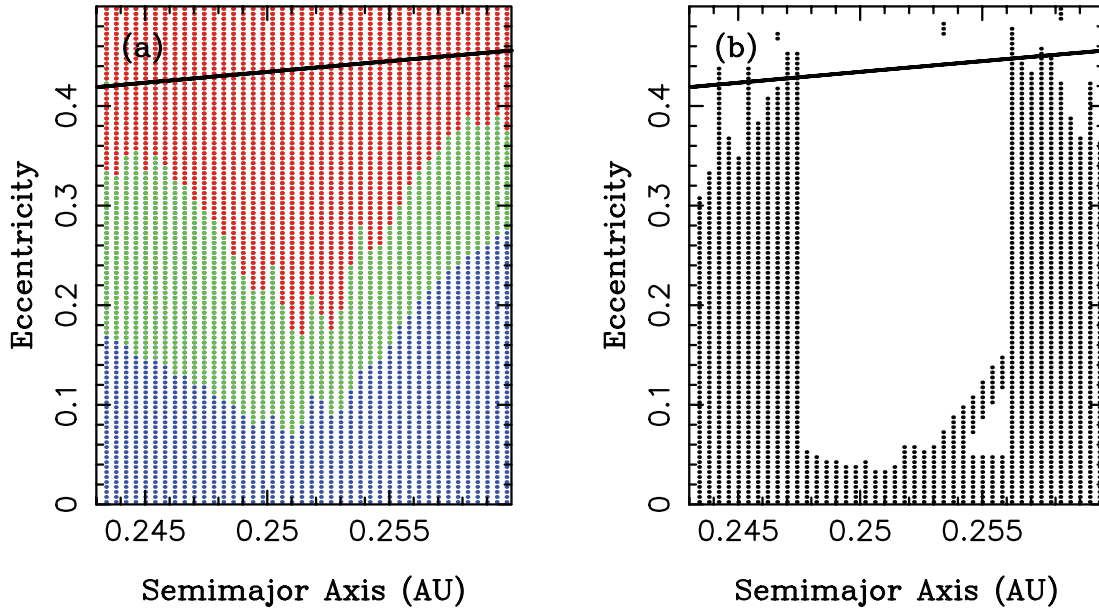


FIG. 7.—Zoom in of Fig. 4 near the 4 : 1 planetary resonance. We used  $f_{\text{cut}} = 0.1$  here. The gap in (b) shows the problematic region where our nominal PT method fails to produce the correct TTV signal.

The residual short-period signal can then be modeled by the PT method as in the nonresonant case (see Figs. 6b and 8). Finally, using the *resonant* perturbation theory (currently in development) or *N*-body integrations, it must be verified that the identified resonant solutions match both the short- and long-period resonant harmonics seen in the TTV signal.

#### 4. DETERMINATION OF $m_2$ , $a_2$ , AND $e_2$ FROM TTVs

Here we describe how the PT method can be used to determine the mass and orbital parameters of the perturbing planet from TTVs. We first use the Bulirsh-Stoer integrator to produce a synthetic TTV signal for the selected planetary system,  $(\delta t_j)_{\text{synth}}$ , where  $1 \leq j \leq N$  and  $N$  is the number of transits. In all cases discussed

here we assume that the orbit of the inner transiting planet is known (from photometric and radial velocity measurements). Specifically, we set  $a_1 = 0.1$  AU and  $e_1 = 0$ . We then apply the PT method to a large set of the perturbing planet’s parameters and use the least-squares method to determine which parameters best fit the original synthetic TTV signal. Finally, the best-fit solutions are compared to the values of  $m_2$ ,  $a_2$ , and  $e_2$  that we used to generate TTVs in the numerical integration.

The following tests were performed with  $m_0 = M_{\text{Sun}}$ ,  $T_{\text{int}} = 1000$  days (producing  $N = 87$  consecutive primary transits of the inner planet) and coplanar orbits of the two planets. In addition to the three basic parameters that we would like to know in this case,  $m_2$ ,  $a_2$ , and  $e_2$ , the TTV signal also depends on three additional

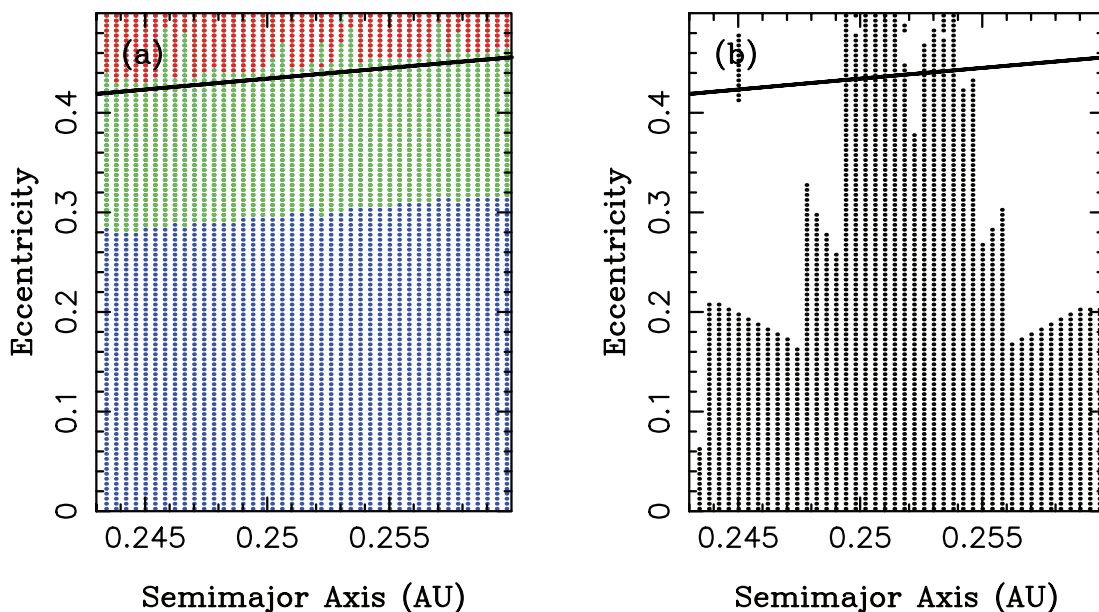


FIG. 8.—Same as Fig. 7, but based on frequencies  $>2\pi/100 \text{ day}^{-1}$ . (b) shows that the PT method is capable of reproducing the short-period oscillations of the TTV signal in the resonance. Therefore, by isolating the short-period TTV harmonics and analyzing them separately with the PT method, we achieve satisfactory precision of the analysis in a domain that is complementary to Fig. 7b.

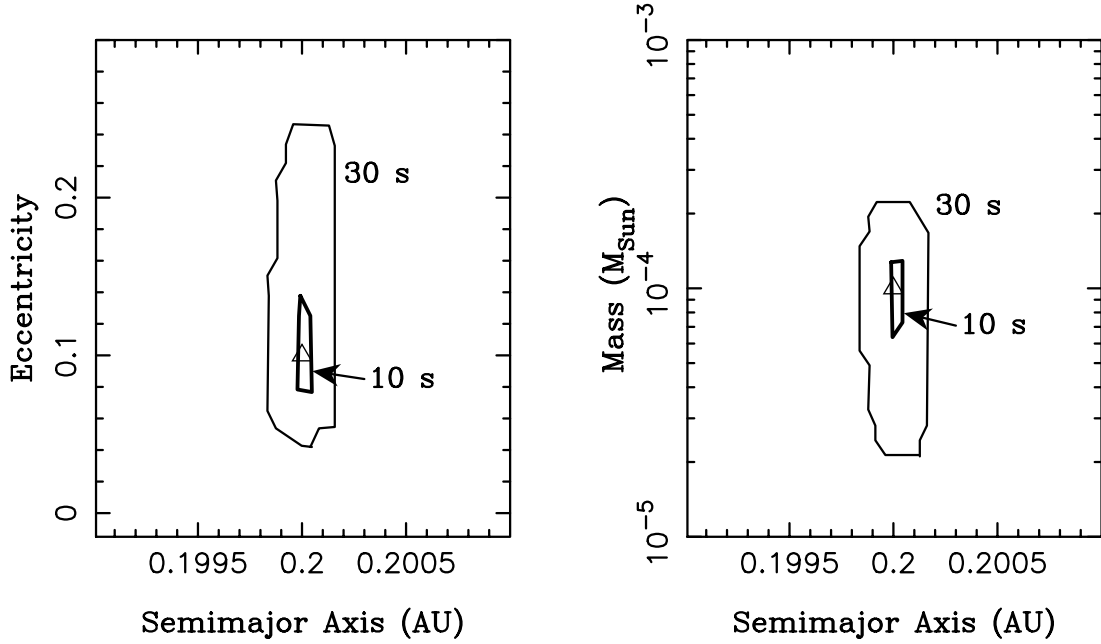


FIG. 9.—Best-fit parameters obtained by the least-squares fit to 87 transit times for our case-1 planetary system (see Fig. 1). The parameters of the perturbing planet are denoted by triangles ( $m_2 = 10^{-4}m_0$ ,  $a_2 = 0.2$  AU, and  $e_2 = 0.1$ ). The thick and thin lines show the envelopes of solutions for  $\eta_{\text{cut}} = 10$  s and  $\eta_{\text{cut}} = 30$  s, respectively.

unknown parameters, namely the mean and pericenter longitudes of the outer perturbing planet,  $\lambda_2^{(0)}$  and  $\varpi_2^{(0)}$ , both defined for a fixed epoch, and the pericenter precession rate,  $g_2 = d\varpi_2/dt$ . We include  $g_2$  here as a free parameter to account for the nongravitational effects (e.g., star's oblateness, relativity, and tides) and those produced by secular interaction between planets.<sup>6</sup>

Ideally, we would like to fit for all six parameters described above. In reality, however, the full sampling of parameter space with six dimensions would be CPU time consuming and not convenient for testing purposes. In the first set of tests, we therefore fix  $\lambda_1 = \lambda_2 = \varpi_2 = 0$  at the first transit, set  $g_2 = 0$ , and fit for  $m_2$ ,  $a_2$ , and  $e_2$  only. Specifically, we searched for solutions with  $10^{-5}m_0 < m_2 < 10^{-2}m_0$ ,  $0.11 < a_2 < 1.0$  AU, and  $e_2 < 0.6$ . Since we found that a fine resolution in  $a_2$  is needed to converge to the correct solution, we used 8000 values of  $a_2$ . Parameters  $m_2$  and  $e_2$  were sampled by 100 and 60 points, respectively. In total, nearly 50 million planetary systems were tracked by the PT method, requiring about 10 minutes of the CPU time on our Opteron-246 computer (i.e.,  $\sim 10^5$  systems are tracked per second). In comparison, our efficient  $N$ -body integrator tracks 1 planetary system over  $T_{\text{int}} = 1000$  days in about 0.1 s. Therefore, the speed up factor that we obtain by using the PT method is  $\sim 10^4$ . The results obtained from the three-parameter fits are described in § 4.1.

In the second set of experiments, we fit for  $m_2$ ,  $a_2$ ,  $e_2$ ,  $\lambda_2^{(0)}$ , and  $\varpi_2^{(0)}$  where  $\lambda_2^{(0)}$  and  $\varpi_2^{(0)}$  are defined as the values of the mean and pericenter longitudes at the first transit. These five-parameter fits are more CPU consuming. We therefore used only a rough resolution in  $\lambda_2^{(0)}$  and  $\varpi_2^{(0)}$ . Specifically, we sampled these angles by 36 values that were evenly spread over  $360^\circ$ . Given the results described in § 4.2 below, the  $10^\circ$  resolution of  $\lambda_2^{(0)}$  and  $\varpi_2^{(0)}$  appears to be adequate. In each of our five-parameter tests, more than  $6 \times 10^{10}$  planetary systems were followed, requiring about a week of the CPU time.

<sup>6</sup> We do not need to include  $g_1 = d\varpi_1/dt$  as a free parameter because  $e_1$  is assumed to be small.

We applied the above-described procedure to a variety of planetary systems. For brevity, we discuss here only the four representative cases shown in Figures 1–3 and 6b. Two methods were used to produce the best-fit solutions in each case. In the first method, we selected trial values of  $m_2$ ,  $a_2$ , and  $e_2$  and defined

$$\eta^2 = \frac{1}{N} \sum_{j=1}^N [(\delta t_j)_{\text{trial}} - (\delta t_j)_{\text{synth}}]^2, \quad (22)$$

where  $(\delta t_j)_{\text{trial}}$  is the trial  $\delta t$  of the  $j$ th transit. We searched for the minimum of  $\eta$  over all trial values with  $m_2$ ,  $a_2$ , and  $e_2$  placed on a grid as described above. We also defined regions of parameter space where  $\eta < \eta_{\text{cut}}$  with  $\eta_{\text{cut}}$  in seconds. Different cutoff values of  $\eta_{\text{cut}}$  were then tested to help us to understand the effects of instrumental noise on the range of acceptable solutions.

In the second method, we added the white noise with characteristic amplitude  $\sigma_{\text{wn}}$  to  $(\delta t_j)_{\text{synth}}$ .<sup>7</sup> The goal of this exercise was to simulate real observation data,  $(\delta t_j)_{\text{obs}}$ , which can be effected by random (and uncorrelated) instrumental errors with characteristic amplitude  $\sigma_{\text{wn}}$ . We defined

$$\chi^2 = \sum_{j=1}^N \left[ \frac{(\delta t_j)_{\text{trial}} - (\delta t_j)_{\text{obs}}}{\sigma_{\text{wn}}} \right]^2 \quad (23)$$

and searched for the minimum of  $\chi^2$  over all trials. The confidence levels for the normally distributed data were then defined as  $\Delta\chi^2 = \chi^2 - \chi_{\text{min}}^2 < (\Delta\chi^2)_{\text{cut}}$ , where the  $(\Delta\chi^2)_{\text{cut}}$  values were properly chosen for  $N$  and the required confidence level. For example,  $(\Delta\chi^2)_{\text{cut}} = 105$  with  $N = 87$  corresponds to the 95% probability. The corresponding confidence regions of  $m_2$ ,  $a_2$ , and  $e_2$  for different values of  $\sigma_{\text{wn}}$  were inspected. We summarize the results below.

<sup>7</sup> The red noise modeling goes beyond the scope of this paper.

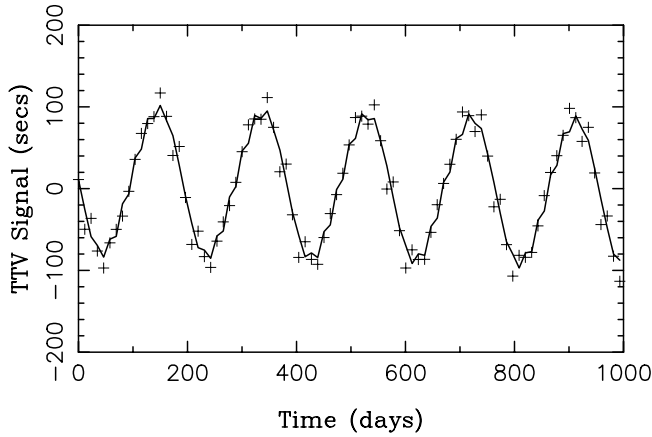


FIG. 10.— Example of the non-uniqueness of the inverse problem. Plus signs show the original TTV signal for our case-1 planetary system ( $a_1 = 0.1$  AU,  $e_1 = 0$ ,  $m_2 = 10^{-4}m_0$ ,  $a_2 = 0.2$  AU, and  $e_2 = 0.1$ ). The solid line shows the TTV signal obtained with  $m_2 = 1.4125 \times 10^{-4}m_0$ ,  $a_2 = 0.15265$  AU, and  $e_2 = 0.03$ . This later solution was identified by the PT method as a fit to the original TTV data with  $\eta = 15.6$  s. The two series of TTVs shown here would therefore be indistinguishable if the uncertainty of the TTV measurements exceeded  $\approx 15$  s.

#### 4.1. Three-parameter Fits

We start by discussing the results based on equation (22). Figure 9 shows the best-fit solutions for case 1 ( $m_2 = 10^{-4}m_0$ ,  $a_2 = 0.2$  AU, and  $e_2 = 0.1$ ). With  $\eta_{\text{cut}} = 10$  s, the least-squares fit identifies the correct mass and orbit of the outer planet with no significant ambiguity.

The uncertainty of determined parameters  $m_2$  and  $e_2$  significantly increases with increasing  $\eta_{\text{cut}}$ . For example, these parameters are constrained only within  $0.04 < e_2 < 0.25$  and  $2 \times 10^{-5} < m_2/m_0 < 2.5 \times 10^{-4}$  for  $\eta_{\text{cut}} = 30$  s. In contrast,  $a_2$  could be determined with an exquisite precision even for  $\eta_{\text{cut}} = 30$  s (Fig. 9). This result stems from the sensitivity of  $n_2$  to the exact value of  $a_2$  and its effects on the behavior of  $\lambda_2$  in the argument of equation (14). For  $\eta_{\text{cut}} > 15$  s, however, additional (incorrect) solutions start to appear as acceptable fits, such as  $m_2 \approx 1.5 \times 10^{-5}m_0$ ,

$a_2 \approx 0.153$  AU, and  $e_2 \lesssim 0.05$  (Fig. 10). Apparently, the inverse problem becomes non-unique for low signal-to-noise ratio (S/N). In particular, the noise can mask TTV harmonics that were crucial for the solution's uniqueness. With  $\eta_{\text{cut}} > 15$  s (in this case), only a few main harmonics can be resolved in TTVs. If that is the case the planet detection can still be achieved by the TTV method, but the characterization of the perturbing planet's parameters becomes ambiguous.

Interestingly, the critical level of  $\eta_{\text{cut}}$  that can ensure a unique (and correct) solution is rather a weak function of the number of transits that we include in our computation. For example, if we decrease the number of transits from the original 87 (corresponding to the continuous 1000 day transit data) to 22 (corresponding to 250 days), the uniqueness threshold does not change much and, in the specific case discussed here, remains at the  $\approx 15$  s level. Figure 11 shows the range of the best-fit orbital parameters for 43 and 22 transits. With only 10 transits (corresponding to 120 days), however, the inverse problem becomes ambiguous even for unrealistically small  $\eta_{\text{cut}}$  of order of a few seconds. We emphasize that these results were obtained with the three-parameter fit. Fits to a larger number of parameters would probably suffer from more ambiguity.

The best-fit solutions from 87 transits of the case-2 planetary system ( $m_2 = 10^{-4}m_0$ ,  $a_2 = 0.32$  AU, and  $e_2 = 0.35$ ) and  $\eta_{\text{cut}} = 10$  s have  $4 \times 10^{-5} < m_2/m_0 < 3 \times 10^{-4}$ ,  $0.3198 < a_2 < 0.3201$  AU, and  $0.26 < e < 0.42$ . This is comfortably close to the original parameters. Incorrect solutions start to appear for  $\eta_{\text{cut}} > 10$  s.

Figure 12 shows the best-fit solutions for case 3 ( $m_2 = 10^{-4}m_0$ ,  $a_2 = 0.15$  AU, and  $e_2 = 0.05$ ) and  $\eta_{\text{cut}} = 100$  s. They nicely match the input parameters. The uncertainty improves when we adopt lower levels of  $\eta_{\text{cut}}$ . For example,  $9 \times 10^{-5} < m_2/m_0 < 1.2 \times 10^{-4}$ ,  $0.1499 < a_2 < 0.1501$  AU, and  $0.03 < e < 0.08$  with  $\eta_{\text{cut}} = 50$  s. Ambiguous solutions arise for  $\eta_{\text{cut}} > 100$  s in this example. Therefore, the threshold value of  $\eta_{\text{cut}}$  in case 3 is about 1 mag larger than those in cases 1 and 2. We conclude that the compact planetary orbits (such as our case 3) can be more easily characterized from TTVs

The resonant case shown in Figure 7 ( $m_2 = 10^{-4}m_0$ ,  $a_2 = 0.25$  AU, and  $e_2 = 0.2$ ) would be more difficult to identify with

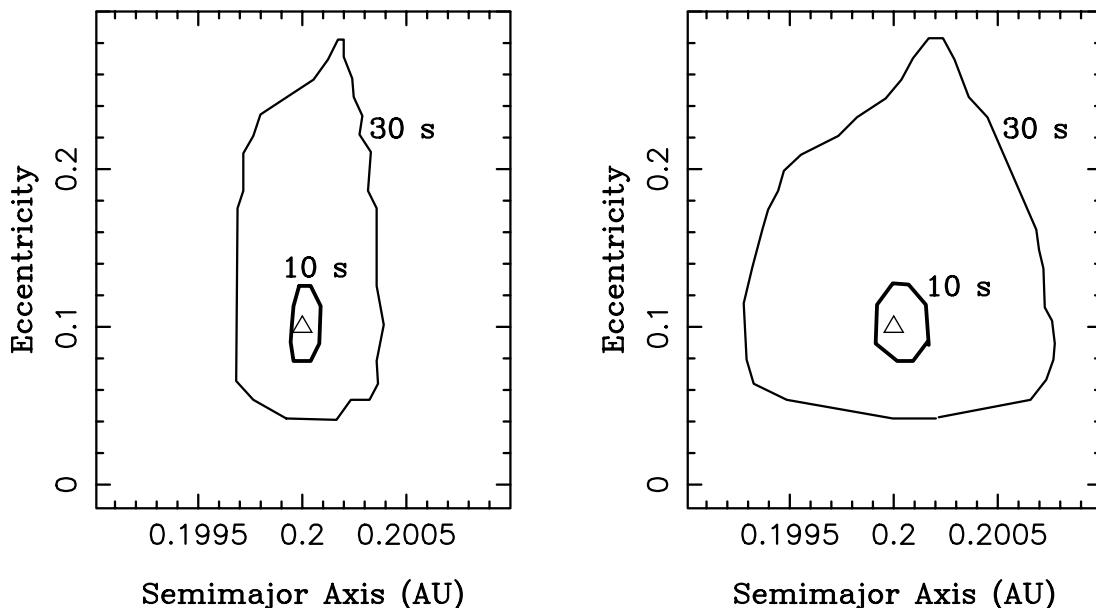


FIG. 11.— Same as Fig. 9, but for 43 (left) and 22 transits (right). This figure demonstrated the increased uncertainty in the determined parameters when small number of transits are available.

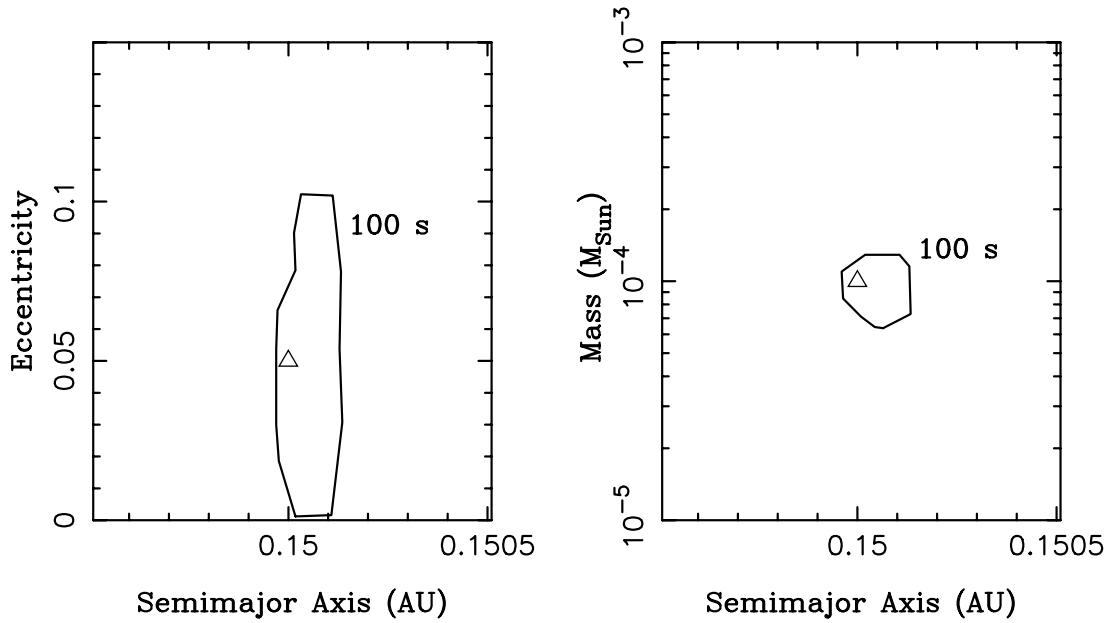


FIG. 12.—Same as Fig. 9, but for our case-3 planetary system (see Fig. 3). The parameters of the perturbing planet, denoted by a triangle in each panel, are  $m_2 = 10^{-4}m_0$ ,  $a_2 = 0.15$  AU, and  $e_2 = 0.05$ . The contour line shows the envelope of solutions with  $\eta_{\text{cut}} = 100$  s.

realistic values of  $\eta_{\text{cut}}$ , because the filtered short-period signal has only a small amplitude. Specifically, we find that with  $\eta_{\text{cut}} = 5$  s the best-fit solution are  $2 \times 10^{-5} < m_2/m_0 < 1.2 \times 10^{-4}$ ,  $0.2485 < a_2 < 0.2505$  AU, and  $e < 0.25$ . Already for  $\eta_{\text{cut}} > 5$  s, however, the PT method is unable to uniquely identify  $a_2$  and picks up a range of incorrect solutions. Therefore, the precision of the TTV measurements better than  $\sim 5$  s would be probably required in this example. (We stress that these issues do not stem from the inaccuracy of the PT method discussed in § 3. Low S/N of the TTV measurements could prevent characterization of the perturbing planet regardless the method used for fitting.)

Finally, we used equation (23) and the appropriate cuts on  $\Delta\chi^2$  to calculate the confidence regions of parameters  $m_2$ ,  $a_2$ , and  $e_2$  for different values of  $\sigma_{\text{wn}}$ . In general, we found that the correct solution can be identified at high confidence levels ( $\geq 99\%$ ) for values of  $\sigma_{\text{wn}}$  that are at least somewhat smaller than the uniqueness thresholds of  $\eta_{\text{cut}}$  established above. For  $\sigma_{\text{wn}}$  exceeding these thresholds, namely  $\sigma_{\text{wn}} > 15, 10, 100$ , and  $5$  s for cases 1, 2, 3, and 4, respectively, the perturbing planet would be difficult to characterize from TTVs alone.

#### 4.2. Five-parameter Fits

The results obtained with the five-parameter fits, where we allowed  $\lambda_2^{(0)}$  and  $\varpi_2^{(0)}$  to vary (in addition to  $m_2$ ,  $a_2$ , and  $e_2$ ), show little difference with respect to those obtained with the three-parameter fits. In general, the region of acceptable fits with  $\eta < \eta_{\text{cut}}$  becomes about a factor of  $\sim 2$  wider in  $a_2$  than that obtained previously (Figs. 9, 11, and 12). This is due to the fact that a slight change in  $a_2$  may be compensated by modifying the values of  $\lambda_2^{(0)}$  and  $\varpi_2^{(0)}$  so that the resulting  $\eta$  value remains roughly unchanged. This mainly affects fits to the TTVs with a short time baseline. Interestingly, we find that the range of the estimated  $m_2$  and  $e_2$  values obtained from the five-parameter fit is similar to that obtained for the three-parameter fit (independently of the length of the TTV time baseline). Therefore, the discussion in § 4.1 of the white noise effects on the results is also valid here.

We found that the values of  $\lambda_2^{(0)}$  and  $\varpi_2^{(0)}$  can be correctly constrained from the data (Fig. 13), although the uncertainty can

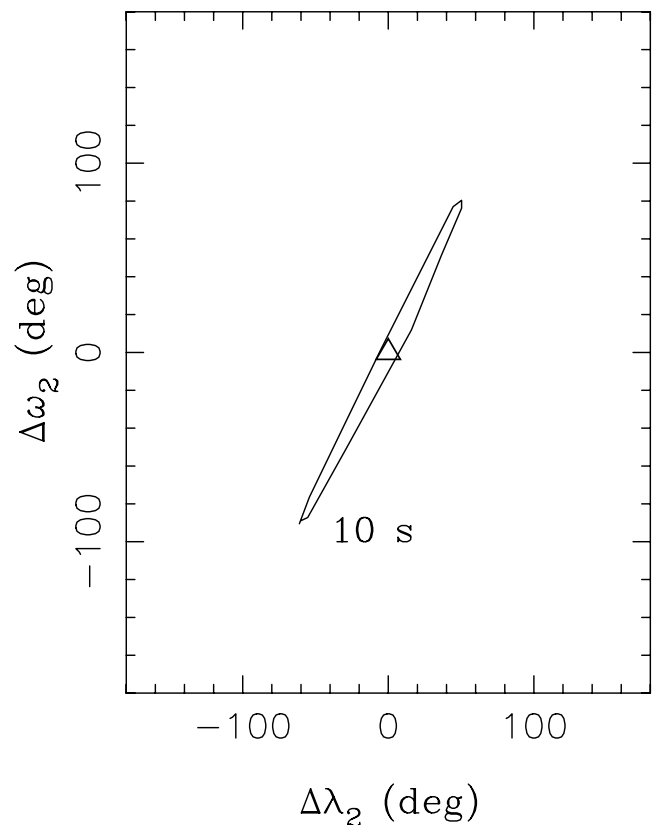


FIG. 13.—Range of acceptable values obtained for our case-1 planetary system (see Fig. 3) with the five-parameter fit. We plot  $\Delta\lambda_2 = \lambda_{2,\text{est}} - \lambda_2^{(0)}$  and  $\Delta\varpi_2 = \varpi_{2,\text{est}} - \varpi_2^{(0)}$ , where  $\lambda_{2,\text{est}}$  and  $\varpi_{2,\text{est}}$  are the estimated values from the five-parameter fit, and  $\lambda_2^{(0)}$  and  $\varpi_2^{(0)}$  are the original values that we used to set up the test. The triangle denotes the best-fit solution. The contour line shows the envelope of solutions with  $\eta_{\text{cut}} = 10$  s.

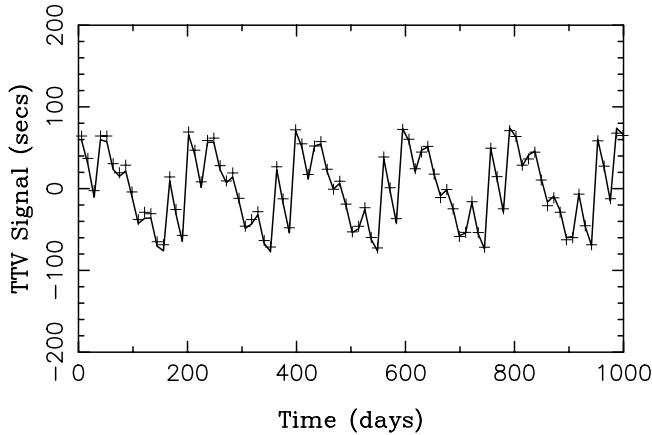


FIG. 14.— Same as Fig. 1, but for the secondary transits. The solid line shows the transit times for the best-fit solution ( $m_2 = 0.97 \times 10^{-4} m_0$ ,  $a_2 = 0.2$  AU, and  $e_2 = 0.102$ ) that we obtained with the PT method from 87 primary and 87 secondary consecutive transits. Plus signs show the secondary transit times for the original parameters ( $m_2 = 10^{-4} m_0$ ,  $a_2 = 0.2$  AU, and  $e_2 = 0.1$ ).

be large. For example, the best-fit values for the case 1 fall dead on the  $\lambda_2^{(0)}$  and  $\varpi_2^{(0)}$  values that we used to set up the test. With  $\eta_{\text{cut}} = 10$  s, however, the estimated values of  $\lambda_2^{(0)}$  and  $\varpi_2^{(0)}$  are spread over a wide range ( $\approx 80^\circ$ ) about the correct solution. There also appears to be strong correlation between the estimated values of  $\lambda_2^{(0)}$  and  $\varpi_2^{(0)}$  with larger values of  $\lambda_2^{(0)}$  corresponding to larger values of  $\varpi_2^{(0)}$  (Fig. 13). Similar correlations were found for all tested planetary systems.

#### 4.3. Secondary Transits

The timing of secondary transits (when the planet passes beyond the star) can also help to detect and characterize the unseen planet in the system. As discussed in Heyl & Gladman (2007), the secondary transits can be especially useful to detect the long-term effects such as the apsidal precession produced by the perturbing planet. Here we concentrate on the effects of the *short-period* variations in the timing of secondary transits.

As in §§ 4.1 and 4.2, we performed tests with  $m_0 = M_{\text{Sun}}$ ,  $a_1 = 0.1$  AU,  $e_1 = 0$ , and  $T_{\text{int}} = 1000$  days (producing 87 primary and 87 secondary transits). Unlike in §§ 4.1 and 4.2, however, we then used *both* the primary and secondary transits to estimate the parameters of the perturbing planet from the PT method. Given the results obtained in § 4.2, which demonstrate that the three- and five-parameter fits are similar, we used the three-parameter method here to economize the CPU time. Below we discuss the results obtained for the four representative cases shown in Figs. 1–3 and 6b.

The envelope of acceptable solutions with  $\eta < \eta_{\text{cut}} = 10$  and 30 s for case 1 is very similar to that shown in Figure 9, where we did not use secondary transits. Figure 14 illustrates our best fit to the 87 secondary transit times (the fit to the 87 primary transit times is very similar to the solid line shown in Fig. 1). When fewer transits are used, we identify trends very similar to those already described in § 4.2 and illustrated in Figure 11. Specifically, the envelope of solutions becomes wider in  $a_2$  and remains about the same in  $m_2$  and  $e_2$ . The results for cases 2, 3, and 4 show the same behavior. Therefore, we conclude that (1) the secondary transits do not help much to improve the precision of results, and (2) the correct solution can be identified with a relatively small number ( $\sim 20$ ) of (primary and/or secondary) transits.

The secondary transits can be very important to ensure the uniqueness of the results. As we discussed in § 4.2, the unique

solution in case 1 was achieved from primary transits alone with  $\eta_{\text{cut}} < 15$  s, assuming that at least  $\sim 20$  primary transits were observed. If, in addition to  $\sim 20$  primary transits, at least  $\sim 20$  secondary transits were also observed, the uniqueness is ensured for  $\eta_{\text{cut}} < 25$  s, thus placing a weaker requirement on the precision of the timing measurements (here we assume that the timing of primary and secondary transits is measured with equal precision). We found a similar increase in the critical  $\eta$  value (by  $\sim 50\%$ – $100\%$ ) in cases 2, 3, and 4. Therefore, observations of secondary transits can be very important to achieve a unique determination of the perturbing planet parameters from the TTVs.

#### 4.4. Gaps in Transit Observations

Above we assumed that observations of the *consecutive* transit times are available. This is generally not the case of real observations where long delays may occur between different sets of telescopic observations and/or transits may be observed with a diluted sampling. We tested such effects by introducing artificial gaps in our synthetic TTV series, by sampling every second, third, or fourth consecutive transit, etc. We found that the total number of observed transits, rather than their time distribution, determines whether or not a unique and correct solution can be identified from the short-period timing variations of transits. A longer time base of transit observations can be important to characterize the resonant and long-period components in the TTV signal.

## 5. CONCLUSIONS

Above we discussed our attempts to determine the parameters of the perturbing planet by the least-squares fit to the TTV signal. We found that the PT method can sample the parameter space about  $10^4$  times faster than the  $N$ -body integrations. The white noise threshold that allows for unique and correct solutions of the inverse problem varies from case to case but is typically a small fraction ( $\sim 15\%$ – $30\%$ ) of the full TTV amplitude. Therefore, while the planet detection can be achieved from TTVs with relatively large  $\sigma_{\text{wn}}$  values, the determination of the planet's parameters is a more delicate problem and may require very high precision measurements.

What is the optimal observing strategy to characterize a planetary system from the TTVs? Based on the tests described in § 4, we observe that (1) the high-precision measurements of at least  $\sim 20$  transits (primary or secondary) are generally needed to ensure the uniqueness of the results; (2) if  $\geq 20$  transits were observed, it may be beneficial to dilute the sampling and look for the long-term trends in the timing of (ideally both) the primary and secondary transits such as the ones produced by the resonant and long-period effects; (3) observations of secondary transits can be very useful to achieve the uniqueness as they help to increase the sampling frequency of the diagnostic short-period variations in the signal; (4) the total number of the observed transits (rather than their time distribution) is central to the inversion process; and (5) the very high precision measurements will be needed to characterize a planetary system with small perturbing planets.

The PT method discussed in this paper can be generalized to account for (1) eccentric orbit of the transiting planet, and (2) planetary systems with inclined orbits. Improved precision near the mean motion resonances can be achieved by using a higher-order perturbation theory. The problem with the divergence of the Laplacian expansion for high eccentricities can be resolved by using the Beaugé's expansion (Beaugé 1996) of the disturbing function, which is valid even for crossing planetary orbits. Moreover, efficient minimum-seeking methods (such as

the genetic algorithm, “simulated annealing” method, etc.; e.g., Beaugé et al. 2008) can be implemented in the algorithm to search for the best-fit solutions rather than using a simple grid technique used here. These developments are left for future work.

This work was supported by the National Science Foundation. We thank Dimitri Veras, who helped us with Figure 5. We also thank David Charbonneau, Daniel Fabrycky, Darin Ragozzine, and Jeremy Heyl for their comments on this work.

## REFERENCES

- Agol, E., & Steffen, J. H. 2007, *MNRAS*, 374, 941  
Agol, E., Steffen, J., Sari, R., & Clarkson, W. 2005, *MNRAS*, 359, 567  
Beaugé, C. 1996, *Celest. Mech. Dyn. Astron.*, 64, 313  
Beaugé, C., Giuppone, C. A., Ferraz-Mello, S., & Michtchenko, T. A. 2008, *MNRAS*, 385, 2151  
Brouwer, D., & Clemence, G. M. 1961, *Methods of Celestial Mechanics* (New York: Academic Press)  
Deprit, A. 1969, *Celest. Mech.*, 1, 12  
Ellis, K. M., & Murray, C. D. 2000, *Icarus*, 147, 129  
Gladman, B. 1993, *Icarus*, 106, 247  
Heyl, J. S., & Gladman, B. J. 2007, *MNRAS*, 377, 1511  
Holman, M. J., & Murray, N. W. 2005, *Science*, 307, 1288  
Hori, G. 1966, *PASJ*, 18, 287  
Kaula, W. M. 1962, *AJ*, 67, 300  
Morbidei, A. 2002, *Modern Celestial Mechanics: Aspects of Solar System Dynamics* (London: Taylor & Francis)  
Press, W. H., Teukolsky, S. A., Vetterling, W. T., & Flannery, B. P. 1992, *Numerical Recipes in FORTRAN: The Art of Scientific Computing* (Cambridge: Cambridge Univ. Press)  
Šidlichovský, M. 1990, *Bull. Astron. Inst. Czech. Acad. Sci.*, 42, 116  
Steffen, J. H., & Agol, E. 2005, *MNRAS*, 364, L96  
Sundman, K. F. 1916, *Öfversigt Finska Vetenskaps-Soc. Förh.*, 58 A, 24  
Torres, G., Winn, J. N., & Holman, M. J. 2008, *ApJ*, 677, 1324